ELSEVIER

Contents lists available at ScienceDirect

# Journal of Hazardous Materials

journal homepage: www.elsevier.com/locate/jhazmat





# Effect of single and multilayered Ti<sub>3</sub>C<sub>2</sub>T<sub>X</sub> MXene as a catalyst and adsorbent on enhanced sonodegradation of diclofenac and verapamil

Sewoon Kim <sup>a</sup>, Seong-Nam Nam <sup>b</sup>, Chang Min Park <sup>c</sup>, Min Jang <sup>d</sup>, Nadar Taheri-Qazvini <sup>e, f</sup>, Yeomin Yoon <sup>a, \*</sup>

- a Department of Civil and Environmental Engineering, University of South Carolina, 300 Main Street, Columbia, SC 29208, USA
- b Department of Civil Engineering, Korea Army Acamemy at Yeong-Cheon, 495 Hogook-ro, Kokyungmeon, Yeong-Cheon, Gyeongbuk 38900, Republic of Korea
- <sup>c</sup> Department of Environmental Engineering, Kyungpook National University, 80 Daehak-ro, Buk-gu, Daegu 41566, Republic of Korea
- d Department of Environmental Engineering, Kwangwoon University, 20 Kwangwoon-Ro, Nowon-Gu, Seoul 01897, Republic of Korea
- e Department of Chemical Engineering, University of South Carolina, Columbia, SC 29208, USA
- <sup>f</sup> Biomedical Engineering Program, University of South Carolina, Columbia, SC, 29208, USA

#### ARTICLE INFO

#### Keywords: Ti<sub>3</sub>C<sub>2</sub>T<sub>X</sub> MXene Pharmaceuticals Ultrasonics Catalyst Adsorption

#### ABSTRACT

Single and multilayered  $Ti_3C_2T_X$  MXene (referred to as SLM and MLM in this study, respectively) was applied as catalysts in the ultrasonic (US) process to treat selected pharmaceutical compounds including diclofenac and verapamil (VRP). Due to solid surface, elemental composition, and functional groups of  $Ti_3C_2T_X$  MXene, the free OH• production was increased by 48.8% for the US treatment with SLM and 59.8% for the US treatment with MLM compared with the US-only treatment. Additionally, adsorption affected the performance during the US treatment in the presence of the catalyst. Thus, the US treatment in the presence of  $Ti_3C_2T_X$  MXene had an enhanced performance not only because of increased oxidation but also because of adsorption, particularly between positively charged VRP and negatively charged  $Ti_3C_2T_X$  MXene. Moreover, although the degradation of the performance was higher for SLM (85.1%) than for MLM (81.8%), by improving the dispersion and reducing the size via sonication, the US treatment in the presence of MLM showed the highest synergy effect. In other words, the US treatment in the presence of MLM showed higher performance than the simple sum of oxidation and adsorption. These findings confirm that the US treatment in the presence of MLM may be a promising technology to treat various pharmaceuticals as a more degradable, strongly reusable, and less toxic process.

# 1. Introduction

Over the past decades, the development of technology has resulted in significant improvements across multiple industries. The pharmaceutical industry has experienced advances in particular because health is one of the most important domains of society (Hester et al., 2020). Consequently, not only can people have adequate access to medicines but associated chemicals can also be easily discharged into the environment. Accordingly, analytical technologies have advanced, increasing our detection capabilities, and researchers are widely discussing the tracing of pharmaceuticals present in wastewater, groundwater, surface water, and drinking water (Bexfield et al., 2019; Luo et al., 2014). For example, the centers for disease control and prevention have reported sharply increasing antibiotic use at acute care hospitals of 1115 in 2018; 1496 in 2019; 1934 in 2020, and 2140 in 2021 (CDC,

2021). Additionally, studies have reported that these chemicals raise concerns regarding their potential risk to people, even at levels of nanograms to micrograms. Nevertheless, conventional water and wastewater processes were not designed to optimize the removal efficiencies of pharmaceuticals because pharmaceuticals have different physicochemical properties than normal contaminants and are detected at low levels (Bai et al., 2018; Kim et al., 2018). Westerhoff et al. reported that coagulants or softening removed < 25% of pharmaceuticals and chlorine removed < 10% of pharmaceuticals in a simulated water treatment plant (Westerhoff et al., 2005). Additionally, according to a recent United States Geological Survey report in 2019, 844 public drinking water sources contained at least one pharmaceutical compound (Bexfield et al., 2019). These data demonstrate that trace pharmaceuticals are a contemporary water issue.

Among the numerous promising technologies available, ultrasonic

E-mail address: yoony@cec.sc.edu (Y. Yoon).

 $<sup>^{\</sup>ast}$  Corresponding author.

(US) techniques are popular for treating organic contaminants because of their extremely short reaction time, efficient degradation of organic compounds having various physicochemical properties, and easy operation (Nie et al., 2021). Organic contaminants, including pharmaceuticals, are degraded by powerful oxidants (OH $^{\bullet}$ :  $E^{\circ} = 2.80 \text{ V}$ ;  $HO_2^{\bullet}$ :  $E^{\circ} =$ 1.70 V; and  $O^{\bullet}$ :  $E^{\circ} = 2.42 \text{ V}$ ) through the pyrolysis of water molecules during US treatment (Colmenares et al., 2014). The dissociation of the water molecules results from the three steps of acoustics cavitation: bubble formation, bubble growth (unstable size), and the implosive collapse of cavitation bubbles (Segura et al., 2012). During this process, the temperature and pressure inside the cavitation bubbles reach ~5000 K and ~1000 atm, respectively, for an instant, resulting in thermally dissociated water molecules. Furthermore, depending on the physicochemical properties of the target organic contaminants, these contaminants react in the three different bubble zones: the gaseous region, the gas-liquid transition region, and the bulk liquid phase. Commonly, because of the high temperatures involved, hydrophobic and volatile contaminants are degraded in the gaseous region via pyrolysis (Park et al., 2011). Moderate hydrophobic and nonmoderate volatile contaminants and hydrophilic and nonvolatile contaminants are degraded in the gas-liquid transition region and the bulk liquid phase, respectively, by reactive oxidation species (Im et al., 2013).

With these advantages of US treatment, supporting materials, such as sonocatalysts, have been applied to accelerate the degradation rate in recent years. Sonocatalysts in the US process act as additional nuclei, resulting in the enhanced pyrolysis of water molecules and free radical production. Additionally, sonocatalysts play the role of an adsorbent, resulting in increased removal efficiency. Diverse materials have been used to improve the US treatment performance, as described in Table S1. Particularly, because of their unique properties, two-dimensional (2D) materials have been applied in the oxidation treatment area (Wang et al., 2019, 2021; Xie et al., 2021). Ti<sub>3</sub>C<sub>2</sub>T<sub>X</sub> MXene is a very new 2D material family that has been investigated at the beginning step to the sonodegradation area. Because of its strong hydrophilicity, tunable structure, and high metallic conductivity, Ti<sub>3</sub>C<sub>2</sub>T<sub>X</sub> MXene has a huge potential as both a sonocatalyst and an adsorbent in US technology (Jeon et al., 2021). However, so far, research concerning Ti<sub>3</sub>C<sub>2</sub>T<sub>X</sub> MXene as a catalyst still lacks diversity in terms of both material and performance studies.

Therefore, synthesized single and multilayered Ti<sub>3</sub>C<sub>2</sub>T<sub>X</sub> MXene (referred to as SLM and MLM, respectively, in this study) was evaluated as both catalysts and adsorbents to treat pharmaceuticals during US treatment. A globally available pain and inflammation reliever, diclofenac (DCF), and a common high blood pressure and angina controller, verapamil (VRP) were selected as the target pharmaceuticals. The H<sub>2</sub>O<sub>2</sub> production rate and degradation kinetics of the selected compounds were studied during US reactions at two different US frequencies (28 and 570 kHz) in the absence and presence of Ti<sub>3</sub>C<sub>2</sub>T<sub>X</sub> MXene. Additionally, the performance was compared for a US-only treatment, US treatments in the presence of Ti<sub>3</sub>C<sub>2</sub>T<sub>X</sub> MXene, and US treatments in the presence of Ti<sub>3</sub>C<sub>2</sub>T<sub>X</sub> MXene adsorption on the basis of the synergetic index. Furthermore, the performance was investigated under various water quality conditions such as different solution pH values, temperatures, and US power densities and the existence of natural organic matter (NOM) and OH promoters and scavengers. For a practical view of this system, a reusability test of the Ti<sub>3</sub>C<sub>2</sub>T<sub>X</sub> MXene catalyst was carried out by examining the removal performance and an X-ray diffraction (XRD) characterization. Additionally, the performance based on the dissolved organic carbon (DOC) was evaluated to confirm the mineralization effect. Lastly, a possible mechanism for US treatment with and without the Ti<sub>3</sub>C<sub>2</sub>T<sub>X</sub> MXene catalyst is proposed.

#### 2. Experimental

# 2.1. Chemicals and analyses of the target pharmaceuticals and $H_2O_2$ production

To prepare  $Ti_3C_2T_X$  MXene,  $Ti_3AlC_2$  powders were purchased from Carbon-Ukraine (Warminster, PA, USA). Lithium fluoride (LF, >99.99%) and hydrofluoric acid (HF, 48%) were obtained from Sigma-Aldrich (St. Louis, MO, USA).

As the target pharmaceuticals, DCF and VRP were purchased from Sigma-Aldrich; Table S2 summarizes the physicochemical properties of these pharmaceuticals. To evaluate the performance under various water qualities, the pH was adjusted with 0.1 M HCl and NaOH solutions. Additionally, humic acid (HA) as an NOM, carbon tetrachloride (CCl<sub>4</sub>) as an OH $^{\bullet}$  promotor, and methanol (MeOH) as an OH $^{\bullet}$  scavenger were obtained from Sigma-Aldrich. The pharmaceutical samples were analyzed using high-performance liquid chromatography (HPLC) (1200 series, Agilent Technologies, Santa Clara, CA, USA) with a fluorescence detector. The target pharmaceuticals were placed in a 2 mL amber vial for the HPLC analysis. All samples were filtered using a 0.22  $\mu$ m syringe filter. A 5  $\mu$ m column (Atlantis T3; Waters, Milford, MA, USA) was used at a flow rate of 1.2 mL/min with a 100  $\mu$ L injection volume. The mobile phase was a 60:40 (v/v) mixture of acetonitrile and phosphoric acid (5 mM)

To measure the evolved amount of  $H_2O_2$  production, the KI dosimetry method was applied using ammonium molybdate tetrahydrate ( $\geq 99.98\%$ ), potassium iodide (99%), and potassium hydrogen phthalate ( $\geq 99.95\%$ ). The chemicals were purchased from Sigma-Aldrich and an ultraviolet–visible spectrophotometer (DR6000, Hach, Loveland, CO, USA) at a wavelength of 350 nm was used for the  $H_2O_2$  determination.

# 2.2. Fabrication and physicochemical characterization of $Ti_3C_2T_X$ MXene

 $Ti_3C_2T_X$  MXene was fabricated as in our previous studies (Kim et al., 2021a). During this fabrication process, 1.56 g of LiF was dissolved in 20 mL of an HCl (9 M) solution to prepare the etching solution. Then, 1 g of  $Ti_3AlC_2$  MAX powder was gradually added to the solution under magnetic stirring at 45 °C for 28 h. The resulting dispersion was washed with deionized (DI) water and centrifuged several times until the desired pH was between 5 and 6. The unreacted  $Ti_3AlC_2$  powder was separated from the dispersion in this step. Finally, the dispersion was centrifuged again to separate it into SLM and MLM. The SLM and MLM were dried to obtain powders; Fig. 1a describes the fabrication process of these materials.

XRD (D/max-2500, Rigaku, Tokyo, Japan) was used to confirm the crystal structure of the prepared materials, and the crystallinity of the XRD patterns was used to evaluate their reusability. Additionally, dynamic light scattering (Zetasizer Nano ZS, Malvern Instruments, Westborough, MA, USA) was applied to obtain the size distribution of the synthesized  $\rm Ti_3C_2T_X$  MXene flakes. The chemical composition and bonds of the prepared  $\rm Ti_3C_2T_X$  MXene were evaluated via X-ray photoelectron spectroscopy (XPS; Quantera SXM, ULVAC-PHI, Japan) and Fourier–transform infrared spectroscopy (FT-IR, Frontier, PerkinElmer, USA). Finally, transmission electron microscopy (TEM; Titan G2, FEI, Hillsboro, OR, USA) and atomic force microscopy (AFM; XE-200, Park Systems, Suwon, KOR) were used to visualize the size and morphologies and to confirm the structure of the prepared materials, respectively.

# 2.3. US experiment

For the US treatment experiment, a rectangular parallel piped stainless-steel reactor (having a length (L) of 15 cm, a depth (D) of 10 cm, and a height (H) of 20 cm) with a frequency generator (Ultech, Daegu, Korea) with transducers at the bottom and a water jacket was used. The desired temperature was controlled by the water jacket using a circulator (Fisher Scientific Inc., Pittsburgh, PA, USA). To optimize the

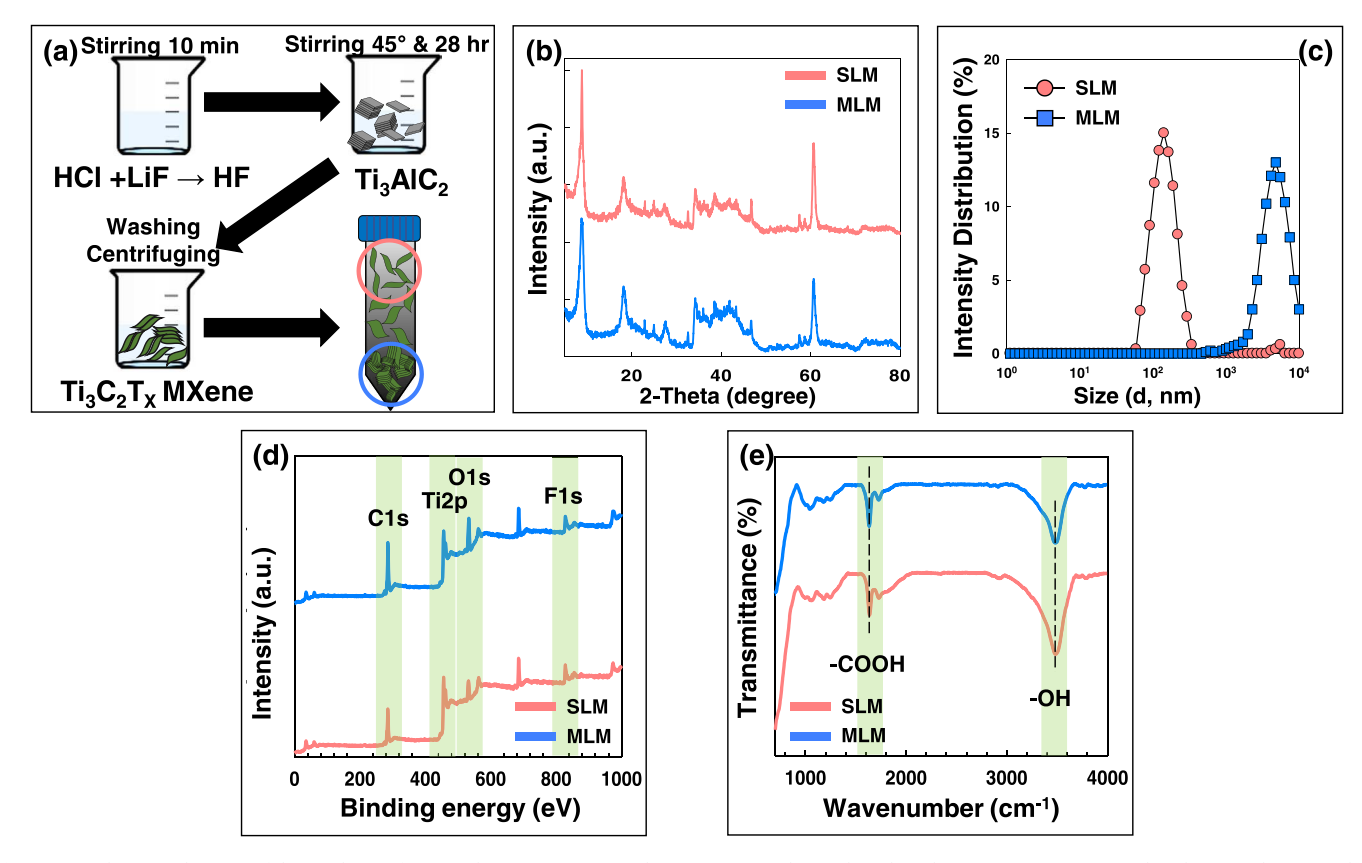


Fig. 1. (a) Schematic diagram of the synthesis of SLM and MLM. Comparison between SLM and MLM based on (b) XRD patterns, (c) size distribution, (d) XPS, and (e) FT-IR.

US frequency and the effect of the catalyst, experiments were conducted under different US frequencies (28 and 570 kHz) and catalyst concentrations (0, 5, 15, and 45 mg/L) with a fixed US power density (180 W/L) for both DCF and VRP. Additionally, to enable a more precise comparison of the catalyst effect, the synergetic index value was calculated according to Eq. (1).

$$Synergetic \quad index = \frac{k_1 \quad (US \quad combined \quad with \quad Catalyst)}{k_1 \quad (US \quad only) \quad + \quad k_1 \quad (Catalyst \quad only)} \tag{1}$$

Here, the  $k_1$  value is the degradation rate constant of the pseudo-first-order kinetic model. To test various water quality effects, the performance under various water qualities was tested with different pH values (3.5, 7, and 10.5), temperatures (283, 293, 303, and 313 K), HA concentrations (2.5, 5, and 10 mg/L), power densities (90, 135, 180, and 225 W/L), oxidation promotors (1, 5, and 25 mM), and oxidation scavengers (1, 5, and 25 mM).

### 3. Results and discussion

# 3.1. Characterization and H<sub>2</sub>O<sub>2</sub> formation effects of SLM and MLM

Before testing the effect of  $Ti_3C_2T_X$  MXene as a sonocatalyst, the crystalline phase, flake size distribution, elemental compositions, and existing functional groups of the synthesized  $Ti_3C_2T_X$  MXene were evaluated, as shown in Fig. 1. The XRD patterns, with peaks near  $9^\circ$  and  $60^\circ$ , agree with previous reports (Lukatskaya et al., 2013; Mashtalir et al., 2013). Additionally, a relatively lower intensity for MLM than for SLM was observed in the diffraction profile. This is attributed to untreated MAX (i.e., the amorphous phase) included in the precipitated MLM, resulting in deconstructive scattering (Munoz-Senmache et al., 2020). The size of SLM ranges from 58.8 to 342 nm, with an average size of 142 nm. Conversely, MLM ranged from 631 to 10,000 nm, with an

average size of 4800 nm. The data indicate that as a promising method of controlling the size of  $\rm Ti_3C_2T_X$  MXene, centrifugation distinguishes different densities of  $\rm Ti_3C_2T_X$  MXene (Maleski et al., 2018). Furthermore, the analyzed XPS and FT-IR data were in agreement with previous studies (Liu et al., 2019; Meng et al., 2018). Particularly, the F and O elements and the –COOH and –OH functional groups on the termination of the prepared materials were demonstrated via XPS and FT-IR, respectively, indicating the possibility of an improved oxidation process as a catalyst. Lastly, the TEM images and AFM thicknesses (Fig. S1) confirmed and identified the larger size of MLM compared with SLM. Altogether, these observations indicate that both SLM and MLM are well made and have great potential as sonocatalysts.

Fig. 2 shows the  $H_2O_2$  production in the absence or presence of  $Ti_3C_2T_X$  MXene as a sonocatalyst during US treatments at 28 and 570 kHz. US treatment results in the decomposition of water into  $OH^{\bullet}$  and  $H^{\bullet}$  at the initial stage, as described in Eq. (2). After the initial stage,  $H^{\bullet}$  and dissolved  $O_2$  are reacted, resulting in the generation of  $HO_2^{\bullet}$  (Eq. (3)). Furthermore, by recombining two  $HO_2^{\bullet}$  (Eq. (4)) and two  $OH^{\bullet}$  (Eq. (5)),  $H_2O_2$  is formed in the aqueous phase.

$$H_2O$$
 (sonolysis)  $\rightarrow$   $H^{\bullet} + OH^{\bullet}$   $k_1 = unknwon$  (2)

$$H^{\bullet} + O_2 \rightarrow HO_2^{\bullet} \quad k_2 = 2.1 \times 10^{10} \quad M^{-1} \quad S^{-1}$$
 (3)

$$HO_2^{\bullet} + HO_2^{\bullet} \rightarrow H_2O_2 + O_2 \quad k_3 = 8.3 \times 10^5 \quad M^{-1} \quad S^{-1}$$
 (4)

$$OH^{\bullet} + OH^{\bullet} \rightarrow H_2O_2 \quad k_4 = 5.5 \times 10^9 \quad M^{-1} \quad S^{-1}$$
 (5)

The amount of produced reactive oxidant species (OH $^{\bullet}$ ) plays an important role in oxidation processes such as US treatments because the degradation efficiency depends on the OH $^{\bullet}$  production (Im et al., 2014). In this process, the produced OH $^{\bullet}$  concentration is primarily dependent on the produced H<sub>2</sub>O<sub>2</sub> concentration because the  $k_4$  value is much higher than the  $k_3$  value based on Eqs. (4) and (5). Thus, the H<sub>2</sub>O<sub>2</sub>

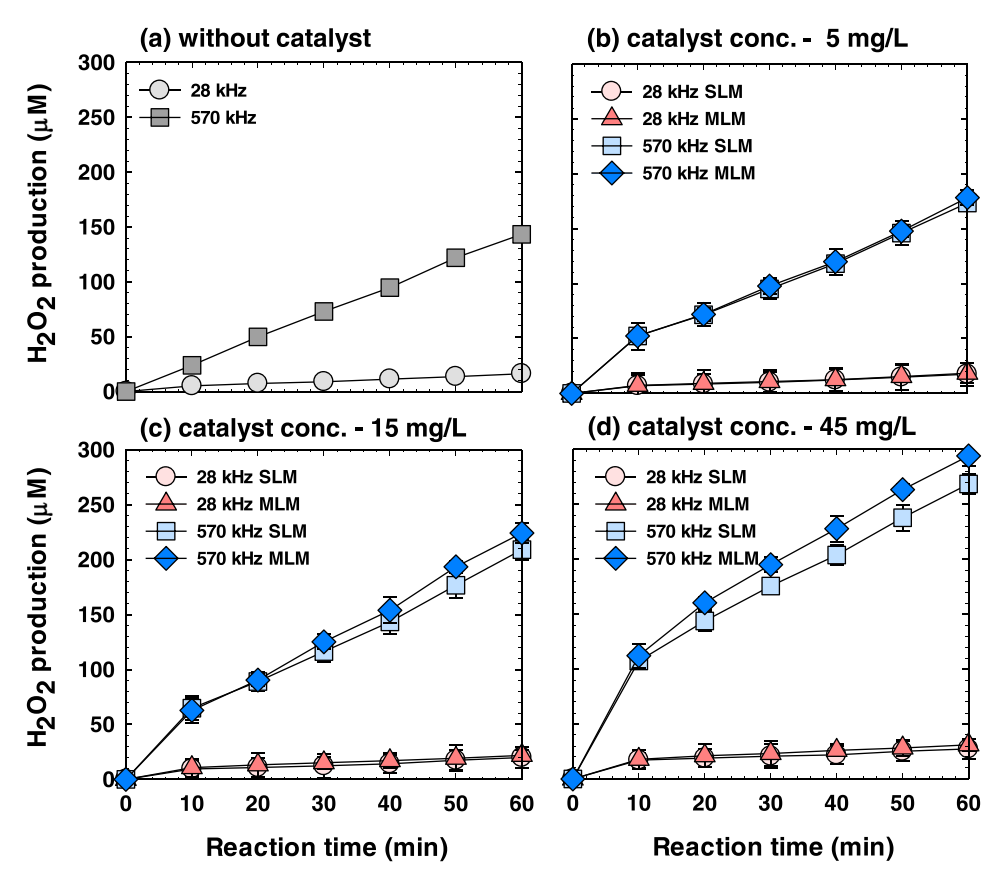


Fig. 2. Production of  $H_2O_2$  on (a) US only treatment, (b) US in the presence of 5 mg/L catalyst, (c) US in the presence of 10 mg/L catalyst, and (d) US in the presence of 45 mg/L catalyst. Operating conditions: pH = 7; US power intensity = 180 W/L.

concentration represents the production of OH (Kormann et al., 1988). The H<sub>2</sub>O<sub>2</sub> production continuously increased with increasing reaction time from 0 to 60 min and increasing catalyst dose from 0 to 45 mg/L. During the H<sub>2</sub>O<sub>2</sub> variation, the initial pH was decreased to less than 1 pH unit. The performance at 570 kHz was significantly higher than that at 28 kHz with or without a catalyst. This is because the intensity and formation of cavitation bubbles promoted even higher production at 570 kHz than at 28 kHz, ejecting a larger fraction of OH production into the bulk solution (Dionisio et al., 2019). Additionally, smaller amounts of cavitation bubbles with a relatively larger size and a short lifetime occurs at lower US frequencies, whereas larger amounts of cavitation bubbles with a smaller size and long lifetime are generated at higher US frequencies (Al-Hamadani et al., 2017; Balachandran et al., 2016). Smaller cavitation bubbles can result in higher H<sub>2</sub>O<sub>2</sub> production by increasing the chances of recombination and formation between H<sup>o</sup> and OH\*. Furthermore, although there was not a significant difference in the production for the US treatment without a catalyst (16.1 µM at 28 kHz and  $143 \,\mu\text{M}$  at  $570 \,\text{kHz}$ ), the US treatment with  $5 \,\text{mg/L}$  of the catalysts (17.5  $\mu$ M for SLM and 18.3  $\mu$ M for MLM at 28 kHz; 174  $\mu$ M for SLM and 178 µM for MLM at 570 kHz), and the US treatment with 15 mg/L of the catalysts (19.9 µM for SLM and 21.8 µM for MLM at 28 kHz;  $209 \,\mu\text{M}$  for SLM and  $224 \,\mu\text{M}$  for MLM at  $570 \,\text{kHz}$ ), the production was considerably enhanced for the US treatment with 45 mg/L of the catalysts (27.3  $\mu M$  for SLM and 31.1  $\mu M$  for MLM at 28 kHz;  $269~\mu M$  for SLM and  $294~\mu M$  for MLM at 570 kHz). These results imply that the presence of Ti<sub>3</sub>C<sub>2</sub>T<sub>X</sub> MXene improves the formation rate of OH<sup>•</sup> production. Additionally, the number of cavitation bubbles increased as a result of the existing rough solid surface, leading to an improved dissociation of the water molecules and free OH production in the US treatment (Jeon et al., 2021). Furthermore, the catalyst acted as additional nuclei, and it was easier to perform water molecule pyrolysis, resulting in increased OH production (Al-Hamadani et al., 2018).

Finally, the  $\rm H_2O_2$  production with  $\rm Ti_3C_2T_X$  MXene catalysts in the US treatment was compared to other US treatment studies with various catalysts, as shown in Table S1. These data show that by exhibiting a high  $\rm H_2O_2$  production performance,  $\rm Ti_3C_2T_X$  MXene as a sonocatalyst was verified as having a strong potential for organic contaminant degradation. The sonocatalyst dose of 45 mg/L was selected for further investigations to obtain optimum performance.

#### 3.2. Sonodegradation of pharmaceuticals by SLM and MLM

The removal rate of DCF and VRP was evaluated in the absence or presence of the sonocatalysts with frequencies of 28 and 570 kHz, as illustrated in Fig. 3. The performance was clearly better at 570 kHz than at 28 kHz under all conditions. As previously mentioned, this is attributed to the higher production of free OH $^{\bullet}$  at 570 kHz than at 28 kHz. Additionally, the free OH $^{\bullet}$  production at this higher frequency reacts relatively easily with contaminants in the bulk liquid phase rather than recombining and forming two OH radicals (Al-Hamadani et al., 2018; Hassani et al., 2017). Furthermore, both contaminants were removed more in the presence of Ti<sub>3</sub>C<sub>2</sub>T<sub>X</sub> MXene. The F and O elements, as well as –COOH, and –OH functional groups, on the surface of Ti<sub>3</sub>C<sub>2</sub>T<sub>X</sub> MXene promote free OH $^{\bullet}$  production, resulting in accelerated degradation (Im et al., 2020). To quantify the required H<sub>2</sub>O<sub>2</sub> concentration, the following stoichiometric calculations were applied:

$$C_{14}H_{11}Cl_2NO_2 \quad (DCF) + 33H_2O_2 \rightarrow 14CO_2 + 37H_2O + HNO_3 + 2HCl$$
 (6)

$$C_{27}H_{38}N_2O_4 \quad (VRP) + 74H_2O_2 \rightarrow 27CO_2 + 92H_2O + 2HNO_3$$
 (7)

According to Eqs. (6) and (7), 165 and 370  $\mu$ M  $H_2O_2$  are required to completely degrade 5  $\mu$ M of DCF and 5  $\mu$ M of VRP, respectively. At 28 kHz, because the produced  $H_2O_2$  was much less than the required

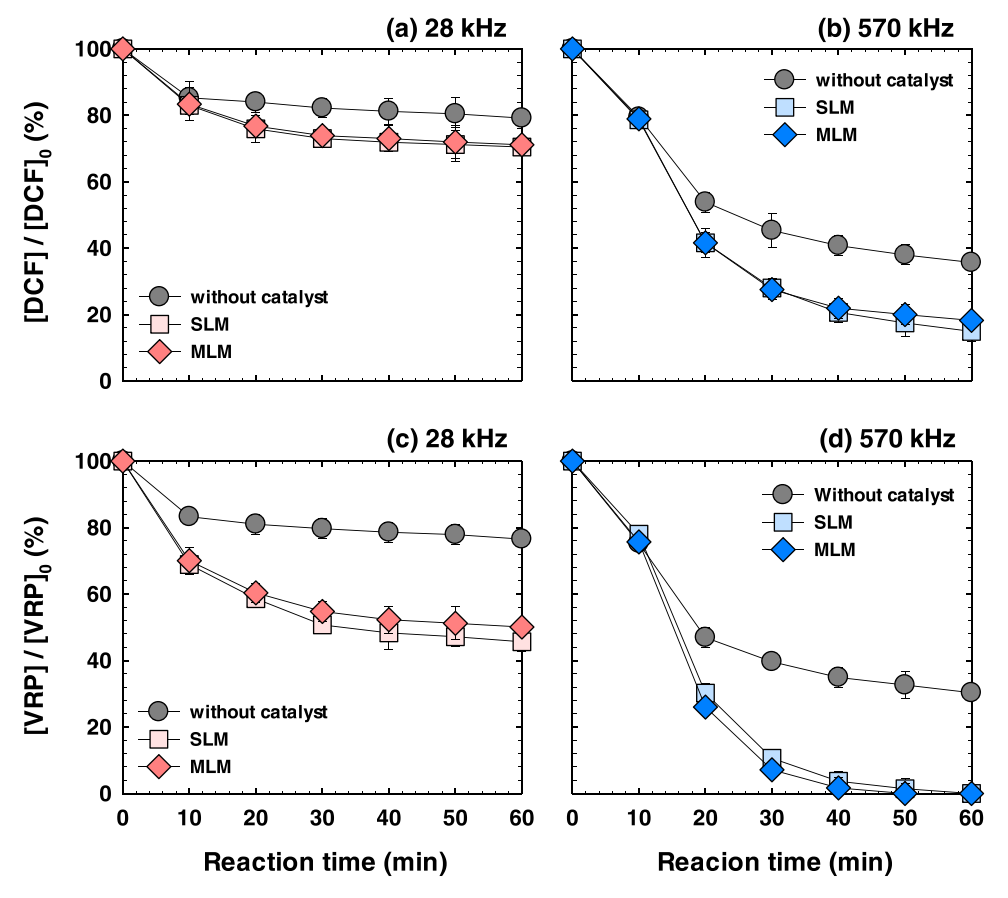


Fig. 3. Degradation of DCF at (a) 28 kHz and (b) 570 kHz, and VRP (c) 28 kHz and (d) 570 kHz in the absence or presence of catalyst as a function of reaction time. Operating conditions: initival [DCF] and [VRP] =  $5 \mu M$ , catalyst =  $45 \mu M$ , catalyst =  $45 \mu M$ , catalyst =  $45 \mu M$ .

 $\rm H_2O_2$ , DCF and VRP showed relatively low removal rates of 20.8% and 23.5% for no catalyst, 29.6% and 54.3% for SLM, and 28.9% and 49.9% for MLM, respectively. At 570 kHz, although the produced  $\rm H_2O_2$  was higher than the required  $\rm H_2O_2$ , DCF was not fully removed at rates of 64.3% for no catalyst, 85.1% for SLM, and 81.8% for MLM. Conversely, for VRP, there was a relatively small gap between the produced and required  $\rm H_2O_2$ , resulting in the complete removal of VRP at 570 kHz. These results are explained by the fact that the measured  $\rm H_2O_2$  concentration did not precisely indicate the amount of free OH radicals during the US treatment. In other words, the  $\rm H_2O_2$  production underestimates the OH $^{\bullet}$  production based on Eqs. (8) and (9).

$$H_2O_2 + OH^{\bullet} \rightarrow H_2O + HO_2^{\bullet} \quad k_5 = 2.7 \times 10^7 \quad M^{-1} \quad S^{-1}$$
 (8)

$$H_2O_2 + H^{\bullet} \rightarrow H_2O + OH^{\bullet} \qquad k_6 = 9.0 \times 10^7 \quad M^{-1} \quad S^{-1}$$
 (9)

These equations show that  $H_2O_2$  reacts with  $OH^{\bullet}$  and  $H^{\bullet}$  as a free radical scavenger, resulting in a negative effect on the  $H_2O_2$  concentration (Dong et al., 2018). Additionally, volatile and/or hydrophobic organic contaminants are degraded in not only the gas–liquid transition region and the bulk liquid phase but also inside the cavitation bubble via direct pyrolysis during the US treatment (Isariebel et al., 2009; Suslick, 1990). Although both VRP and DCF have nonvolatile properties (vapor pressure =  $4.2 \times 10^{-9}$  and  $6.14 \times 10^{-8}$  mm Hg and Henry's law constant =  $8.8 \times 10^{-25}$  and  $4.73 \times 10^{-12}$  atm m³/mol, respectively), VRP (log Kow = 5.04 and water solubility = 13.8 mg/mL) is relatively more hydrophobic than DCF (log Kow = 4.00 and water solubility = 15.1 mg/mL). That is, there might have been an enhanced chance of the degradation of VRP. Furthermore,  $Ti_3C_2T_X$  MXene acts as a sonocatalyst as well as an adsorbent during US treatment. At pH 7, because DCF (strongest acidic pKa = 4.23) was deprived of protons and VRP (strongest basic pKa = 9.68) was protonated with amine groups, their species

were negatively charged and positively charged, respectively (Kim et al., 2021b). Ti $_3$ C $_2$ T $_X$  MXene has a strong negative surface because of its termination consisting of –OH, –H, and/or –F, as shown in Fig. 1. Thus, via electrostatic attraction, positively charged VRP molecules are more adsorbed on Ti $_3$ C $_2$ T $_X$  MXene than negatively charged DCF, resulting in a higher removal rate of VRP.

# 3.3. Evaluation of the synergetic index for US treatments with a catalyst

In the previous sections, we observed that  ${\rm Ti}_3{\rm C}_2{\rm T}_{\rm X}$  MXene demonstrates a strongly improved sonodegradation of the target pharmaceuticals as a sonocatalyst. However, the adsorption effect was still unclear during the US treatment. Accordingly, US-only, US with  ${\rm Ti}_3{\rm C}_2{\rm T}_{\rm X}$  MXene, and  ${\rm Ti}_3{\rm C}_2{\rm T}_{\rm X}$  MXene adsorption-only tests were conducted and compared using the pseudo-first-order rate constant ( $k_1$ ), as shown in Table 1. Expectedly, the  $k_1$  values of the US treatment at 570 kHz for VRP were higher than those of the US treatment at 28 kHz for DCF, respectively. Moreover, adding  ${\rm Ti}_3{\rm C}_2{\rm T}_{\rm X}$  MXene enhanced the degradation performance compared with the US-only treatment. Conversely, although the

**Table 1** Pseudo-first-order rate constant  $(k_1)$  and synergistic index value.

		DCF		VRP	
Values	Processes	28 kHz	570 kHz	28 kHz	570 kHz
$k_1$ (x min <sup>-1</sup> )	US only	0.040	0.072	0.040	0.072
	US + SLM	0.071	0.080	0.071	0.101
	US + MLM	0.069	0.089	0.077	0.128
	SLM adsorption	0.029		0.033	
	MLM adsorption	0.025		0.031	
Synergsitic index	US + SLM	0.962	0.789	0.969	0.961
	US + MLM	0.984	0.915	1.09	1.24

 $k_1$  values of VRP were still higher than those of DCF for both adsorbents for the  $\rm Ti_3C_2T_X$  MXene adsorption-only treatment, lower  $k_1$  values of the adsorption were obtained than for the US treatments in the absence or presence of the materials. These results indicated that the US treatment impacted the removal of the target compounds more than adsorption in the US treatment with the  $\rm Ti_3C_2T_X$  MXene process. Furthermore,  $\rm Ti_3C_2T_X$  MXene improves the degradation performance as a catalyst during US treatment, resulting in a better performance of the US treatment in the presence of  $\rm Ti_3C_2T_X$  MXene.

 $Ti_3C_2T_X$  MXene, as a sonocatalyst including SLM and MLM, was used to enhance the performance of the US treatment in this study. Thus, to compare the effects of the two catalysts, the synergetic index was calculated for the two target compounds and the two frequencies during the US treatment. If the index value is bigger than 1, this indicates that the US treatment combined with the  $Ti_3C_2T_X$  MXene process is superior to the sum of the US-only treatment and the  $Ti_3C_2T_X$  MXene adsorption-only treatment, i.e., the synergistic effect. The  $k_1$  values of SLM were higher than those of MLM for all systems, whereas the synergetic index

values of the US treatment with MLM (0.984 at 28 kHz and 0.915 at 570 kHz for DCF; 1.09 at 28 kHz and 1.24 at 570 kHz for VRP) were higher than those with SLM (0.962 at 28 kHz and 0.789 at 570 kHz for DCF; 0.969 at 28 kHz and 0.961 at 570 kHz for VRP). Particularly, the synergetic index of the US treatment in the presence of MLM for VRP had values higher than 1. These results reflect the fact that the dispersion effect by sonication for MLM was stronger than that for SLM, which help prevent MLM agglomeration (Al-Hamadani et al., 2015). In other words, the sonication effect for SLM, such as the decreasing particle size and increasing dispersion, is less than that for MLM because SLM already had smaller and better-dispersed properties than MLM. Additionally, the dispersion of MLM by the US treatment leads to increasing not only the specific surface area for adsorption sites but also the negatively charged surface area, resulting in higher adsorption with positively charged VRP. Kim et al. reported that sonicated MLM showed an enhanced adsorption performance because of its increased hydrodynamic diameter and its more negatively charged surface (Kim et al., 2021b). Conversely, the synergy indices, except for the US treatment with MLM for VRP, were

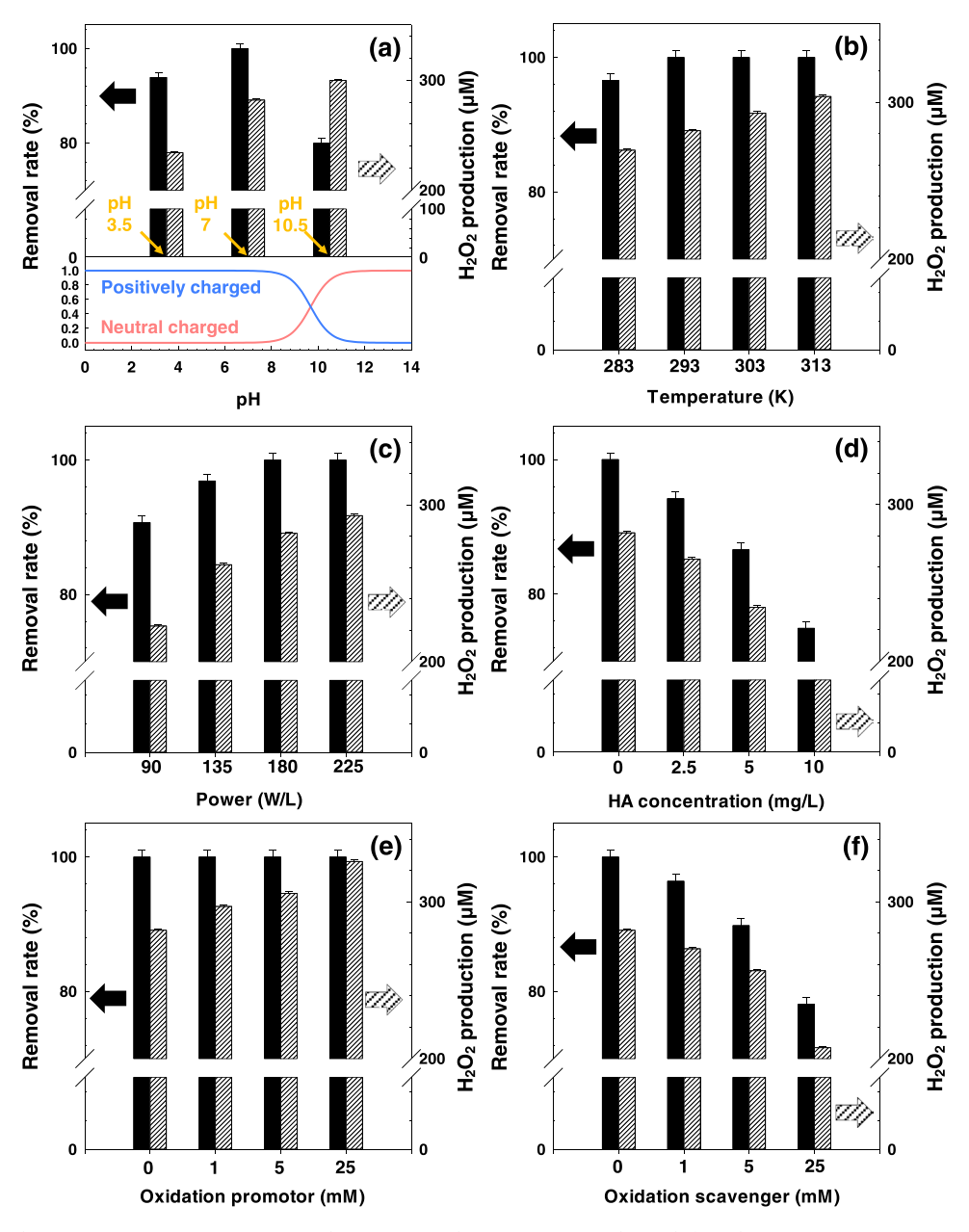


Fig. 4. Effect of (a) pH, (b) temperature, (c) power intensity, (d) NOM, (e) oxidation promoter (CCl<sub>4</sub>), and (f) oxidation scavenger (MeOH) on US performance in the presence of MLM performance. Operating conditions: initial [VRP] =  $5 \mu$ M; MLM = 45 mg/L; reaction time = 60 min.

less than 1. This indicates that the US treatment affects the retrieval of the adsorbed target compounds during this process (Tao et al., 2020). For these reasons, although SLM showed a higher adsorption performance than MLM, the lowest synergetic index of the US treatment with SLM for DCF at 507 kHz was indicated when detaching the adsorbed compounds at the higher frequency. Thus, the US treatment in the presence of the MLM process resulted in greater indices than the sum of both the US and adsorption technologies, acting as a catalyst and an adsorbent.

# 3.4. Effect of various water quality on pharmaceutical degradation and $H_2O_2$ formation

# 3.4.1. Effect of water quality on pharmaceutical degradation and $H_2O_2$

Because there are various water conditions in the real environment, the effects of the solution pH, temperature, and US power density and the existence of NOM and OH promoters and scavengers were investigated for VRP using the US treatment in the presence of MLM. As shown in Fig. 4a, the H<sub>2</sub>O<sub>2</sub> production was continuously increased from pH 3.5-10, whereas the removal performance was varied depending on the pH conditions (93.9% for pH 3.5, 100% for pH 7%, and 80.0% for pH 10.5). Because the uncombined OH production is the highest at lower pH, the produced OH react more easily with VRP than recombine with OH to H<sub>2</sub>O<sub>2</sub>. Additionally, because the OH production increased at pH 3.5 because of the decomposition of H<sub>2</sub>O<sub>2</sub>, this free radical enhanced the VRP oxidation (Harichandran et al., 2016). Conversely, the highest H<sub>2</sub>O<sub>2</sub> concentration was observed at pH 10.5 because of the more rapid recombination of OH than reactions with VRP (Im et al., 2014). Furthermore, as mentioned above, the hydrophobicities and molecular form of VRP change depending on the pH according to Eq. (10).

$$C_{27}H_{37}N_2O_4^+ + H^+ < basic pK_a$$
 (9.68)  $< C_{27}H_{38}N_2O_4$  (10)

This indicates that because of the electrostatic interaction between the high negative surface charge of MLM and the positive VRP, a higher VRP removal was measured for solutions with pH < pKa. Interestingly, the VRP removal at pH 7 was higher than that at pH 3.5. Because the dominant mechanism is not adsorption but the degradation of the target compounds by the US treatment with MLM, although VRP had similar species at pH 3.5 and 7, a higher amount of produced  $\rm H_2O_2$  resulted in the higher removal of VRP at pH 7.

The effect of the temperature conditions in the solution was evaluated, as indicated in Fig. 4b. The  $\rm H_2O_2$  production showed a gradual increase with increasing temperature. By mitigating the threshold limit of the generated cavitation, which results in a reduced surface tension and liquid viscosity, the amount of cavitation bubbles is increased with increasing solution temperature, resulting in higher  $\rm H_2O_2$  production at higher temperatures (Im et al., 2014, 2015). Nonetheless, 96.6% removal of VRP was observed at 283 K and this increased to approximately 100% above 293 K. The relationship between the rate of reaction and the temperature is expressed by the Arrhenius equation, Eq. (11), and is described in Fig. S2.

$$-\ln k = -\ln A + \frac{E_a}{RT} \tag{11}$$

In this study, the measured apparent activation energy ( $E_a$ ) was  $1.196 \text{ kJ mol}^{-1}$  ( $R^2 = 0.955$ ). This low  $E_a$  value implies a fast transition from the reaction to the products (Mao and Campbell, 2019) and is likely controlled by diffusion (Im et al., 2014). This mechanism indicates that an increased temperature results in the easier migration of the target compounds from the bulk solution to the inside of bubbles, where high OH $^{\bullet}$  concentrations and temperatures exist, leading to more degradation (Nie et al., 2021). However, above the optimum temperature condition, the energy of the cavitation bubble diminishes, causing a decreased reaction of the target contaminants during the collapse of the cavitation bubbles (Ghodbane and Hamdaoui, 2009). Accordingly, a steady

removal performance of VRP above 293 K was obtained because of these positive and negative mechanisms.

Fig. 4c shows the variation of the performance and H<sub>2</sub>O<sub>2</sub> production with different US powers. An increase in the VRP removal and the H<sub>2</sub>O<sub>2</sub> production was observed with increasing US power intensity (90.8% for 90 W/L, 96.9% for 135 W/L, 100% for 180 W/L, and 100% for 225 W/ L). A higher power causes a larger amount of cavitation bubbles, increased temperature and pressure, and an increased chance of collapse between compounds and free radicals (Golash and Gogate, 2012; Karim and Shriwastav, 2020). These phenomena presumably led to the increased removal of VRP. Additionally, because NOM exists in nearly all aquatic environments, the effect of NOM was evaluated and HA, dominant fractions of NOM were selected as NOM, as illustrated in Fig. 4d. The result showed that with increasing HA concentration in the solution, both the removal performance and the H<sub>2</sub>O<sub>2</sub> production linearly decreased: 100% for 0 mg/L, 94.3% for 2.5 mg/L, 86.6% for 5 mg/L, and 74.9% for 10 mg/L. HA, which includes carboxylic and phenolic acids, reacts with free radicals during US treatment, causing these contaminants to degrade (Zhang et al., 2011). This result is consistent with observations of the interruption of oxidation by NOM (Laughrey et al., 2001; Rayaroth et al., 2015).

Lastly, the effect of CCl<sub>4</sub> as an oxidation promoter and MeOH as an oxidation scavenger on the VRP removal rate and H<sub>2</sub>O<sub>2</sub> production were examined to investigate the effectiveness of free OH radicals during US treatment. As shown in Fig. 4e, although VRP removal efficiencies were maintained at approximately 100% for all CCl4 concentrations, the amount of produced H2O2 was enhanced as the CCl4 concentration increased. This is explained by the fact that CCl4 decomposed under US treatment. According to the proposed CCl<sub>4</sub> degradation by US treatment, based on Eqs. (S1)- (S7), as an H • scavenger, CCl4 helps decrease H • in the solution. This strongly inhibits H<sup>o</sup> and OH<sup>o</sup> recombination, resulting in promoted free OH radicals in the solution. In other words, most of the produced free radicals are applied to the degradation of the target compounds. Additionally, Fig. 4f indicates a decreased VRP removal rate and H2O2 production with increasing MeOH concentrations ranging from 0 to 25 mM, i.e., 100%, 96.5%, 89.8%, and 78.2%, respectively. Because 3 mM of H<sub>2</sub>O<sub>2</sub> is required to complete the degradation of 1 mM of MeOH based on Eq. (S8), there is competition between MeOH and VRP to be degraded (Yang et al., 2020). Additionally, the results demonstrate that OH radicals play an important role in US treatments.

# 3.5. Reusability of the sonocatalyst

The reusability of MLM during US treatments must be evaluated from a practical perspective. Thus, a VRP removal test was conducted over four cycles of US treatment with recycled MLM using 1 M HCl, 1 M NaOH, and DI based on a previous study (Kim et al., 2021b). Additionally, after each cycle, the crystallinity of MLM was estimated to confirm the quantitative features of the recycled MLM crystallinity using XRD patterns and Origin software following Eq. (S9). As shown in Fig. 5a, although the degradation of VRP during the US treatment in the presence of MLM gradually decreased with an increased number of reuses of the MLM, the performance still showed a competitive result of 80.9%. Additionally, the data indicate that after the cleaning process, adsorbed VRP was well removed by the MLM with high stability of MLM. This is demonstrated by the small difference in the crystallinity of MLM after each cycle: the crystallinity was 100% for cycle 1, 95.1% for cycle 2, 93.8% for cycle 3%, and 90.9% for cycle 4, as shown in Fig. 5b. However, because the dominant mechanism is enhanced oxidation by a catalyst, MLM as an adsorbent did not have a strong effect on the results. Additionally, cavitation bubbles formed by the sonication caused US irradiation, resulting in a higher VRP desorption because of its whirlpool action (Zhou et al., 2015) and the increased solution temperature (Cornelissen et al., 1997). This means an increased chance of VRP oxidation during the process. These properties are be useful for the application of US treatments in the presence of MLM to remove organic

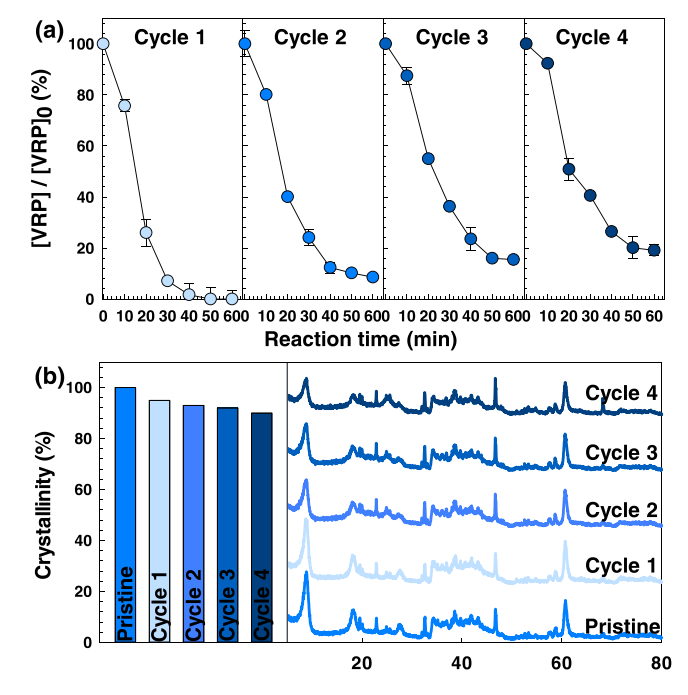


Fig. 5. Evaluation of reusability by (a) VRP degradation over 4 cycles and (b) crystallinity variation. Operating conditions: initial [VRP] = 5  $\mu$ M; MLM = 45 mg/L; pH = 7; US power intensity = 180 W/L.

#### contaminants.

#### 3.6. Mineralization of pharmaceuticals and a possible mechanism

To evaluate the degree of mineralization for VRP, the removal performance was calculated for the US-only treatment, the US treatment in the presence of MLM, and the MLM adsorption-only treatment, as shown in Fig. 6. The removal and removal based on DOC had similar performances for adsorption-only treatment, whereas the removal rates based on DOC were as low as 9% and 15% for the US-only treatment, 9% and 11% for the US treatment with 5 mg/L MLM, 5% and 13% for the US treatment with 15 mg/L MLM, and 4% and 10% for the US treatment with 45 mg/L MLM at 28 and 570 kHz, respectively, than VRP removal on US treatment. This is explained by the formation and accumulation of mineralized VRP during the US treatment. Particularly, at the higher frequency, because of the increased degradation of VRP, a relatively larger gap between removal and removal based on DOC appeared.

Nevertheless, the performance difference decreased with increasing MLM dose because MLM can adsorb both VRP and mineralized VRP. Even the removal based on DOC was 90.1% for the US treatment in the presence of 45 mg/L MLM. These results indicate that although adsorption has a relatively small effect on the performance, it clearly enhanced the performance by adsorbing organic contaminants as well as mineralized contaminants. Furthermore, compared with other oxidation technologies, US treatments are safer because of their lack of chemical by-products (Balachandran et al., 2016; Serna-Galvis et al., 2015). On the basis of these results, a mechanism is proposed for US treatment in the presence of a catalyst. As shown in Fig. 7, not only can adsorption be enhanced by dispersion and a smaller particle size but oxidation can also be improved by MLM because of its termination structure and solid surface.

#### 4. Conclusions

In this study, two types of  $Ti_3C_2T_X$  MXene, SLM, and MLM, were applied as catalysts to treat selected pharmaceutical contaminants, i.e., DCF and VRP, in US treatments at different frequencies. By boosting the  $H_2O_2$  production, the higher frequency (570 kHz) treatment showed better performance than the lower frequency (28 kHz) treatment. Additionally, the US treatment in the presence of a catalyst showed enhanced oxidation because of the highly generated free OH radicals as a result of the rough solid surface, plentiful elements, and functional groups of  $Ti_3C_2T_X$  MXene. These conditions cause a higher degradation of target compounds. Moreover, although the dominant mechanism was oxidation,  $Ti_3C_2T_X$  MXene acted as an adsorbent. Particularly, negatively charged  $Ti_3C_2T_X$  MXene adsorbed more positively charged VRP than DCF. The US treatment in the presence of MLM showed a superior synergetic effect because of the dispersion and decreased surface area of

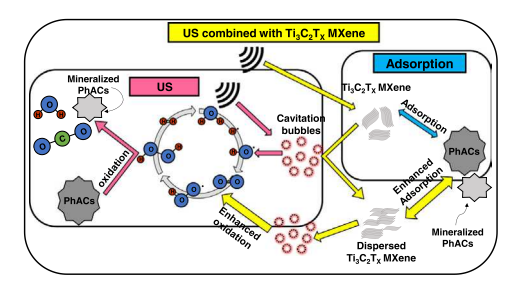
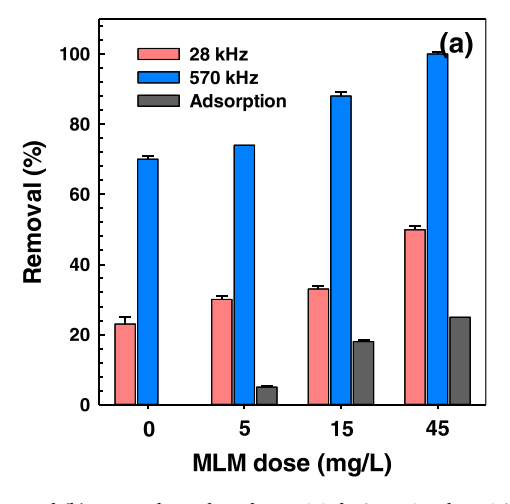


Fig. 7. Proposed mechanism of US only, US in the presence of MLM, and adsorption process only.



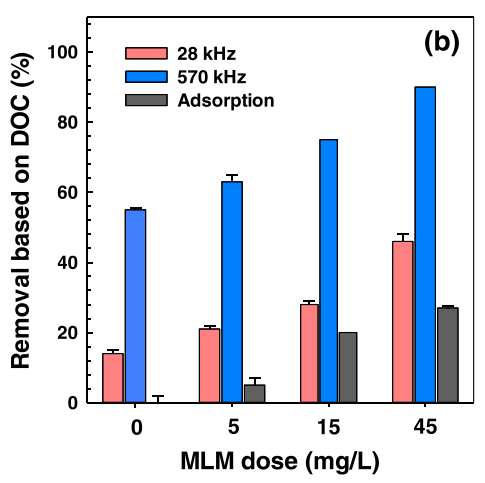


Fig. 6. (a) Removal rate and (b) removal rate based on DOC during US only, US in the presence of MLM, and adsorption only. Operating conditions: initial [VRP]  $= 5 \mu M$ ; pH = 7; US power intensity = 180 W/L; reaction time = 60 min.

MLM resulting from the ultrasound effect. The degradation performance for VRP was measured for different solution pH values, temperatures, sonication powers, HA, oxidation promotors, and scavengers in US treatments in the presence of MLM. On the basis of these experiments, it was confirmed that the solution conditions play an important role in US treatments. In a reusability test,  $\mathrm{Ti}_3\mathrm{C}_2\mathrm{T}_X$  MXene showed a competitive performance after four cycles based on the removal rate and crystal-linity. Additionally, although VRP was mineralized during the US treatment, by acting as both a catalyst and an adsorbent, MLM exhibited good adsorption abilities for both VRP and mineralized VRP. Consequently,  $\mathrm{Ti}_3\mathrm{C}_2\mathrm{T}_X$  MXene may be a suitable sonocatalyst to treat organic contaminants via US treatment in terms of enhanced performance, strong reusability, and reduced toxicity.

### CRediT authorship contribution statement

**Sewoon Kim**: Conceptualization, Investigation, Writing – original draft, Writing – review & editing. **Seong-Nam Nam**: Characterization and writing. **Chang Min Park**: Characterization and writing. **Min Jang**: Sample analyses and writing. **Nader Taheri-Qazvini**: Methodology, Resources. **Yeomin Yoon**: Conceptualization, Supervision, Project administration, Funding acquisition.

#### **Declaration of Competing Interest**

The authors declare that they have no known competing financial interests or personal relationships that could have appeared to influence the work reported in this paper.

#### Acknowledgments

This research was supported by the National Science Foundation, USA (OIA-1632824). This study was also supported by the University of South Carolina ASPIRE program.

## Appendix A. Supporting information

Supplementary data associated with this article can be found in the online version at doi:10.1016/j.jhazmat.2021.128120.

### References

- Al-Hamadani, Y.A., Chu, K.H., Son, A., Heo, J., Her, N., Jang, M., Park, C.M., Yoon, Y., 2015. Stabilization and dispersion of carbon nanomaterials in aqueous solutions: a review. Sep. Purif. Technol. 156, 861–874.
- Al-Hamadani, Y.A., Lee, G., Kim, S., Park, C.M., Jang, M., Her, N., Han, J., Kim, D.-H., Yoon, Y., 2018. Sonocatalytic degradation of carbamazepine and diclofenac in the presence of graphene oxides in aqueous solution. Chemosphere 205, 719–727.
- Al-Hamadani, Y.A., Park, C.M., Assi, L.N., Chu, K.H., Hoque, S., Jang, M., Yoon, Y., Ziehl, P., 2017. Sonocatalytic removal of ibuprofen and sulfamethoxazole in the presence of different fly ash sources. Ultrason. Sonochem. 39, 354–362.
- Bai, X., Lutz, A., Carroll, R., Keteles, K., Dahlin, K., Murphy, M., Nguyen, D., 2018. Occurrence, distribution, and seasonality of emerging contaminants in urban watersheds. Chemosphere 200, 133–142.
- Balachandran, R., Patterson, Z., Deymier, P., Snyder, S.A., Keswani, M., 2016. Understanding acoustic cavitation for sonolytic degradation of p-cresol as a model contaminant. Chemosphere 147, 52–59.
- Bexfield, L.M., Toccalino, P.L., Belitz, K., Foreman, W.T., Furlong, E.T., 2019. Hormones and pharmaceuticals in groundwater used as a source of drinking water across the United States. Environ. Sci. Technol. 53 (6), 2950–2960.
- CDC. 2021. https://www.cdc.gov/antibiotic-use/stewardship-report/current.html.
  Centers for Disease Control and Prevention.
- Colmenares, J.C., Magdziarz, A., Łomot, D., Chernyayeva, O., Lisovytskiy, D., 2014. A new photocatalytic tool in VOCs abatement: Effective synergetic combination of sonication and light for the synthesis of monometallic palladium-containing TiO<sub>2</sub>. Appl. Catal. B-Environ. 147, 624–632.
- Cornelissen, G., van Noort, P.C., Parsons, J.R., Govers, H.A., 1997. Temperature dependence of slow adsorption and desorption kinetics of organic compounds in sediments. Environ. Sci. Technol. 31 (2), 454–460.
- Dionisio, D., Motheo, A., Saez, C., Cañizares, P., Rodrigo, M.A., 2019. Effects of ultrasound irradiation on the electrochemical treatment of wastes containing micelles. Appl. Catal. B-Environ. 248, 108–114.

- Dong, C., Ji, J., Shen, B., Xing, M., Zhang, J., 2018. Enhancement of H<sub>2</sub>O<sub>2</sub> decomposition by the Co-catalytic effect of WS2 on the fenton reaction for the synchronous reduction of Cr (VI) and remediation of phenol. Environ. Sci. Technol. 52 (19), 11297–11308.
- Ghodbane, H., Hamdaoui, O., 2009. Intensification of sonochemical decolorization of anthraquinonic dye Acid Blue 25 using carbon tetrachloride. Ultrason. Sonochem. 16 (4), 455–461.
- Golash, N., Gogate, P.R., 2012. Degradation of dichlorvos containing wastewaters using sonochemical reactors. Ultrason. Sonochem. 19 (5), 1051–1060.
- Hassani, A., Khataee, A., Karaca, S., Karaca, C., Gholami, P., 2017. Sonocatalytic degradation of ciprofloxacin using synthesized TiO<sub>2</sub> nanoparticles on montmorillonite. Ultrason. Sonochem. 35, 251–262.
- Hester, E.T., Lin, A.Y.-C., Tsai, C.W., 2020. Effect of floodplain restoration on photolytic removal of pharmaceuticals. Environ. Sci. Technol. 54 (6), 3278–3287.
- Im, J.-K., Boateng, L.K., Flora, J.R., Her, N., Zoh, K.-D., Son, A., Yoon, Y., 2014. Enhanced ultrasonic degradation of acetaminophen and naproxen in the presence of powdered activated carbon and biochar adsorbents. Sep. Purif. Technol. 123, 96–105.
- Im, J.-K., Heo, J., Boateng, L.K., Her, N., Flora, J.R., Yoon, J., Zoh, K.-D., Yoon, Y., 2013. Ultrasonic degradation of acetaminophen and naproxen in the presence of single-walled carbon nanotubes. J. Hazard. Mater. 254, 284–292.
- Im, J.-K., Yoon, J., Her, N., Han, J., Zoh, K.-D., Yoon, Y., 2015. Sonocatalytic-TiO<sub>2</sub> nanotube, Fenton, and CCl<sub>4</sub> reactions for enhanced oxidation, and their applications to acetaminophen and naproxen degradation. Sep. Purif. Technol. 141, 1–9.
- Im, J.K., Sohn, E.J., Kim, S., Jang, M., Son, A., Zoh, K.-D., Yoon, Y., 2020. Review of MXene-based nanocomposites for photocatalysis. Chemosphere 270, 129478.
- Isariebel, Q.-P., Carine, J.-L., Ulises-Javier, J.-H., Anne-Marie, W., Henri, D., 2009. Sonolysis of levodopa and paracetamol in aqueous solutions. Ultrason. Sonochem. 16 (5), 610–616.
- Jeon, M., Jun, B.-M., Kim, S., Cho, J., Park, C.M., Choong, C.E., Jang, M., Yoon, Y., 2021. Sonodegradation of amitriptyline and ibuprofen in the presence of  $Ti_3C_2T_X$  MXene. J. Hazard. Mater. Lett. 2, 100028.
- Karim, A.V., Shriwastav, A., 2020. Degradation of ciprofloxacin using photo, sono, and sonophotocatalytic oxidation with visible light and low-frequency ultrasound: degradation kinetics and pathways. Chem. Eng. J. 392, 124853.
- Kim, S., Chu, K.H., Al-Hamadani, Y.A., Park, C.M., Jang, M., Kim, D.-H., Yu, M., Heo, J., Yoon, Y., 2018. Removal of contaminants of emerging concern by membranes in water and wastewater: a review. Chem. Eng. J. 335, 896–914.
- Kim, S., Gholamirad, F., Shin, B., Taheri-Qazvini, N., Cho, J., Yu, M., Park, C.M., Heo, J., Yoon, Y., 2021a. Application of a Ti<sub>3</sub>C<sub>2</sub>T<sub>X</sub> MXene-coated membrane for removal of selected natural organic matter and pharmaceuticals. ACS ES&T Water 1 (9), 2164–2173.
- Kim, S., Gholamirad, F., Yu, M., Park, C.M., Jang, A., Jang, M., Taheri-Qazvini, N., Yoon, Y., 2021b. Enhanced adsorption performance for selected pharmaceutical compounds by sonicated  ${\rm Ti}_3{\rm C}_2{\rm T}_X$  MXene. Chem. Eng. J. 406, 126789.
- Kormann, C., Bahnemann, D.W., Hoffmann, M.R., 1988. Photocatalytic production of hydrogen peroxides and organic peroxides in aqueous suspensions of titanium dioxide, zinc oxide, and desert sand. Environ. Sci. Technol. 22 (7), 798–806.
- Laughrey, Z., Bear, E., Jones, R., Tarr, M.A., 2001. Aqueous sonolytic decomposition of polycyclic aromatic hydrocarbons in the presence of additional dissolved species. Ultrason. Sonochem. 8 (4), 353–357.
- Liu, L., Zhao, Q., Liu, R., Zhu, L., 2019. Hydrogen adsorption-induced catalytic enhancement over Cu nanoparticles immobilized by layered  $T_{i3}C_2$  MXene. Appl. Catal. B-Environ. 252, 198–204.
- Lukatskaya, M.R., Mashtalir, O., Ren, C.E., Dall'Agnese, Y., Rozier, P., Taberna, P.L., Naguib, M., Simon, P., Barsoum, M.W., Gogotsi, Y., 2013. Cation intercalation and high volumetric capacitance of two-dimensional titanium carbide. Science 341 (6153), 1502–1505.
- Luo, Y., Guo, W., Ngo, H.H., Nghiem, L.D., Hai, F.I., Zhang, J., Liang, S., Wang, X.C., 2014. A review on the occurrence of micropollutants in the aquatic environment and their fate and removal during wastewater treatment. Sci. Total Environ. 473, 619–641.
- Maleski, K., Ren, C.E., Zhao, M.-Q., Anasori, B., Gogotsi, Y., 2018. Size-dependent physical and electrochemical properties of two-dimensional MXene flakes. ACS Appl. Mater. Interfaces 10 (29), 24491–24498.
- Mao, Z., Campbell, C.T., 2019. Apparent activation energies in complex reaction mechanisms: a simple relationship via degrees of rate control. ACS Catal. 9 (10), 9465–9473.
- Mashtalir, O., Naguib, M., Mochalin, V.N., Dall'Agnese, Y., Heon, M., Barsoum, M.W., Gogotsi, Y., 2013. Intercalation and delamination of layered carbides and carbonitrides. Nat. Commun. 4 (1), 1–7.
- Meng, F., Seredych, M., Chen, C., Gura, V., Mikhalovsky, S., Sandeman, S., Ingavle, G., Ozulumba, T., Miao, L., Anasori, B., 2018. MXene sorbents for removal of urea from dialysate: a step toward the wearable artificial kidney. ACS Nano 12 (10), 10518–10528.
- Muñoz-Senmache, J.C., Kim, S., Arrieta-Pérez, R.R., Park, C.M., Yoon, Y., Hernández-Maldonado, A.J., 2020. Activated carbon-metal organic framework composite for the adsorption of contaminants of emerging concern from water. ACS Appl. Nano. Mater. 3, 2928–2940.
- Nie, G., Hu, K., Ren, W., Zhou, P., Duan, X., Xiao, L., Wang, S., 2021. Mechanical agitation accelerated ultrasonication for wastewater treatment: sustainable production of hydroxyl radicals. Water Res 198, 117124.
- Park, J.-S., Her, N.-G., Yoon, Y., 2011. Sonochemical degradation of chlorinated phenolic compounds in water: effects of physicochemical properties of the compounds on degradation. Water Air Soil Pollut. 215 (1), 585–593.

- Rayaroth, M.P., Aravind, U.K., Aravindakumar, C.T., 2015. Sonochemical degradation of Coomassie Brilliant Blue: effect of frequency, power density, pH and various additives. Chemosphere 119, 848–855.
- Segura, Y., Martínez, F., Melero, J.A., Molina, R., Chand, R., Bremner, D.H., 2012. Enhancement of the advanced Fenton process (Fe<sub>0</sub>/H<sub>2</sub>O<sub>2</sub>) by ultrasound for the mineralization of phenol. Appl. Catal. B-Environ. 113, 100–106.
- Serna-Galvis, E.A., Silva-Agredo, J., Giraldo-Aguirre, A.L., Torres-Palma, R.A., 2015.
  Sonochemical degradation of the pharmaceutical fluoxetine: effect of parameters, organic and inorganic additives and combination with a biological system. Sci. Total Environ. 524, 354–360.
- Suslick, K.S., 1990. Sonochemistry. Science 247 (4949), 1439-1445.
- Tao, Y., Wu, Y., Han, Y., Chemat, F., Li, D., Show, P.L., 2020. Insight into mass transfer during ultrasound-enhanced adsorption/desorption of blueberry anthocyanins on macroporous resins by numerical simulation considering ultrasonic influence on resin properties. Chem. Eng. J. 380, 122530.
- Wang, L., Zhou, G., Luo, H., Zhang, Q., Wang, J., Zhao, C., Rao, A.M., Xu, B., Lu, B., 2019. Enhancing catalytic activity of tungsten disulfide through topology. Appl. Catal. B-Environ. 256, 117802.

- Wang, L., Xie, L., Zhao, W., Liu, S., Zhao, Q., 2021. Oxygen-facilitated dynamic activesite generation on strained MoS2 during photo-catalytic hydrogen evolution. Chem. Eng. J. 405, 127028.
- Westerhoff, P., Yoon, Y., Snyder, S., Wert, E., 2005. Fate of endocrine-disruptor, pharmaceutical, and personal care product chemicals during simulated drinking water treatment processes. Environ. Sci. Technol. 39, 6649–6663.
- Xie, L., Wang, L., Zhao, W., Liu, S., Huang, W., Zhao, Q., 2021. WS2 moiré superlattices derived from mechanical flexibility for hydrogen evolution reaction. Nat. Commun. 12 (1), 1–9.
- Yang, S.-Q., Cui, Y.-H., Li, J.-Y., Lv, X.-D., Liu, Z.-Q., 2020. Determination methods for steady-state concentrations of HO\* and SO<sub>4</sub>\* in electrochemical advanced oxidation processes. Chemosphere 261, 127658.
- Zhang, K., Gao, N., Deng, Y., Lin, T.F., Ma, Y., Li, L., Sui, M., 2011. Degradation of bisphenol-A using ultrasonic irradiation assisted by low-concentration hydrogen peroxide. J. Environ. Sci. 23 (1), 31–36.
- Zhou, C., Gao, N., Li, R., Deng, Y., 2015. Desorption of bisphenol-A (BPA) and regeneration of BPA-spent granular activated carbon using ultrasonic irradiation and organic solvent extraction. Desalin. Water Treat. 54 (11), 3106–3113.